CHIN. PHYS. LETT. Vol. 37, No. 10 (2020) 106102

Structural Domain Imaging and Direct Determination of Crystallographic Orientation in Noncentrosymmetric $Ca_3Ru_2O_7$ Using Polarized Light Reflectance

Guoxiong Tang(唐国雄)[1], Libin Wen(文理斌)[1], Hui Xing(邢晖)[1*], Wenjie Liu(刘文杰)[1], Jin Peng(彭劲)[2], Yu Wang(王瑜)[2,3], Yupeng Li(李宇鹏)[4], Baijiang Lv(吕柏江)[4], Yusen Yang(杨宇森)[1], Chao Yao(姚超)[1], Yueshen Wu(吴越珅)[1], Hong Sun(孙弘)[1], Zhu-An Xu(许祝安)[4], Zhiqiang Mao(毛志强)[2,3], and Ying Liu(刘荧)[3]

[1]*Key Laboratory of Artificial Structures and Quantum Control, and Shanghai Center for Complex Physics, School of Physics and Astronomy, Shanghai Jiao Tong University, Shanghai 200240, China*
[2]*Department of Physics and Engineering Physics, Tulane University, New Orleans 70118, USA*
[3]*Department of Physics, Pennsylvania State University, University Park, PA 16802, USA*
[4]*Zhejiang Province Key Laboratory of Quantum Technology and Device, Department of Physics, Zhejiang University, Hangzhou 310027, China*

(Received 15 July 2020; accepted 19 August 2020; published online 29 September 2020)

The noncentrosymmetricity of a prototypical correlated electron system $Ca_3Ru_2O_7$ renders extensive interest in the possible polar metallic state, along with multiple other closely competing interactions. However, the structural domain formation in this material often complicates the study of intrinsic material properties. It is crucial to fully characterize the structural domains for unrevealing underlying physics. Here, we report the domain imaging on $Ca_3Ru_2O_7$ crystal using the reflection of polarized light at normal incidence. The reflection anisotropy measurement utilizes the relative orientation between electric field component of the incident polarized light and the principal axis of the crystal, and gives rise to a peculiar contrast. The domain walls are found to be the interfaces between 90° rotated twin crystals by complementary magnetization measurements. A distinct contrast in reflectance is also found in the opposite cleavage surfaces, owing to the polar mode of the RuO_6 octahedra. More importantly, the analysis of the contrast between all inequivalent cleavage surfaces enables a direct determination of the crystallographic orientation of each domain. Such an approach provides an efficient yet feasible method for structural domain characterization, which can also find applications in noncentrosymmetric crystals in general.

PACS: 61.50.−f, 71.27.+a, 71.20.Gj, 78.40.Kc DOI: 10.1088/0256-307X/37/10/106102

$Ca_3Ru_2O_7$ is the bilayer member in the layered Ruthenates in Ruddlesden–Popper series family $(Sr,Ca)_{n+1}Ru_nO_{3n+1}$, best known for their rich phase diagrams incorporating exciting physics, including strong ferromagnetism,[1] metamagnetism[2] and metamagnetic texture,[3] electronic nematic phase,[4,5] unconventional superconductivity,[6,7] and band dependent Mott transitions.[8,9] $Ca_3Ru_2O_7$ holds a particular position as it involves competing interactions with comparable energy scales between charge, spin, lattice and orbital degrees of freedoms, resulting in complex phase transitions and an intricate balance susceptible to external perturbations. The system undergoes an antiferromagnetic transition at 56 K and a subsequent first-order structural transition at 48 K.[10] The latter is accompanied by an apparent change in electronic state,[11] noted earlier as a metal-insulating transition, but later found to be correlated with the competing interactions. The underlying mechanism is still under active investigation.[12–14] So far, the consensus is that the ground state of $Ca_3Ru_2O_7$ is an antiferromagnetic semimetal.

The structural instability of $Ca_3Ru_2O_7$ arises due to the smaller size of Ca^{2+} cation, compared to Sr^{2+} cation in the sibling compound $Sr_3Ru_2O_7$.[15] In addition to local rotation around the c axis, the RuO_6 octahedron is also tilted away from the c axis, which breaks the inversion symmetry of the lattice. This leads to a polar lattice that features a ferroelectric order.[16] The combination of a ferroelectric order and a small yet finite carrier density from the semimetallic state makes a polar metal plausible, which is currently in hot pursuit.[17] The lower symmetry also leads to the ubiquitous existence of twined structures in a given crystal, which subsequently creates barriers for probing the intrinsic anisotropic properties of the material. Because the in-plane lattice constants are very close ($a = 5.3781$ Å, $b = 5.5227$ Å), a conventional Laue diffraction cannot differentiate the twined crystals. Earlier studies on anisotropy properties relied on the anisotropic in-plane magnetization measurement as a screening tool, which is capable of identifying the twined crystals.[11,18] However, the spatial distribution of the domains and the crystallographic

Supported by the National Key Research and Development Program of China (Grant Nos. 2019YFA0308602 and 2016YFA0300500), the National Natural Science Foundation of China (Grant Nos. 11804220, 11774305 and 11974237) and Natural Science Foundation of Shanghai (Grant No. 20ZR1428900).
*Corresponding author. Email: huixing@sjtu.edu.cn
© 2020 Chinese Physical Society and IOP Publishing Ltd

orientation of the individual domains are still inaccessible. A more efficient method with a spatial resolution of the structural domain in $Ca_3Ru_2O_7$ is needed, especially for the study of polar metal where spontaneous ferroelectric domains exist.

In this Letter, we report the imaging of structural domain in $Ca_3Ru_2O_7$ by the reflection of polarized light. Clear contrast is observed using an optical microscope in reflectance mode with polarized white light at normal incidence at the crystal surface. The contrast varies with the relative orientation between electric field component of the incident polarized light and the principal axis of the crystal. The corresponding domain walls are found to be at the interfaces between 90°-rotated twin crystals identified by complementary magnetization measurements. More importantly, the opposite cleavage surfaces possess a different color under the same lighting condition, which is due to the polar distortion of the RuO_6 octahedra in this noncentrosymmetric lattice. All inequivalent cleavage surfaces possess distinct colors, which enables a direct determination of the crystallographic orientation of each domain. Our result provides a feasible and efficient approach for structural domain characterization, which can also find applications in layered noncentrosymmetric crystals in general.

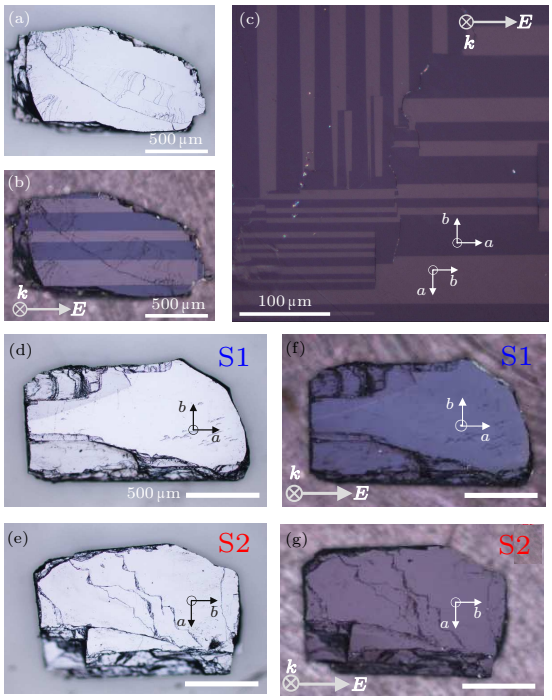

Fig. 1. (a) A typical image of the *ab* plane of $Ca_3Ru_2O_7$ crystal under normal white light. (b) The same crystal under a polarized light at normal incidence, with the electric field of the polarized light parallel to the longer edge of the crystal. (c) The polarized light image of a selected crystal showing features of perpendicular stripes. The arrows indicate the corresponding lattice orientation of the respective regions. Here [(d),(e)] and [(f),(g)] are the images of selected single-domain crystals S1 and S2 under normal white light and polarized light, respectively. Crystallographic orientations in (d)–(g) were identified using magnetization measurements.

$Ca_3Ru_2O_7$ crystals were grown by the floating-zone technique. Preliminary crystal quality was checked using the x-ray diffraction (XRD) and Laue diffraction. The dc magnetic susceptibility was measured with a Quantum Design superconducting interference device magnetometer (SQUID MPMS-5) with fields of up to 5 T. Raman spectra were measured with a Princeton Instruments ARC-SP-2558 spectrometer and a 532 nm laser. All optical images were taken using a Nikon eclipse 80i microscope with polarizer and analyzer in crossed position. The charge density of $Ca_3Ru_2O_7$ is calculated using density functional theory as implemented in the Vienna *ab initio* Simulation package and adopting the project augmented wave potentials. The Perdew–Burke–Ernzerhof functional within the gradient generalized approximation was used.

Figure 1(a) shows a clean smooth surface of $Ca_3Ru_2O_7$ crystal obtained by mechanical cleavage. The crystal exhibits shining black color under ordinary white light due to its metallic nature. However, when the same measurement is performed using a polarized white light with the analyzer in crossed position, a clear contrast appears, as seen in Fig. 1(b). The contrast shows stripe-like shapes in perpendicular relative orientation in a more representative crystal in Fig. 1(c). Considering the orthogonal lattice of $Ca_3Ru_2O_7$, it is likely that these different colored areas correspond to domains from crystal twinning. To verify this, we selected an appropriate crystal showing the contrasts with large enough areas and shape it down to two separate ones, each with one individual color as seen in Figs. 1(d)–1(g) to represent the respective domain. The two crystals are labeled as S1 and S2. As we shall see in the following, the long edges of S1 and S2 are along the crystallographic a and b directions, respectively.

Samples S1 and S2 are used for further structural characterizations. The x-ray diffraction patterns in Fig. 2(a) show that both crystals possess pure bilayer phase. Both the samples also show similar Laue diffraction patterns [Fig. 2(b)]. In the orthogonal lattice of $Ca_3Ru_2O_7$, the in-plane lattice constants are $a = 5.3781$ Å, $b = 5.5227$ Å at room temperature.[15] This 2.6 percent difference between a and b is difficult to be observed in a conventional x-ray Laue diffraction. Raman spectra taken on the two samples are shown in Fig. 2(c). All the observed Raman peaks find good accordance with earlier reported phonon line assignment.[19] No trace of qualitative difference can be found between the Raman spectra of the two samples.

On the other hand, the magnetic anisotropy is rather sensitive to the in-plane crystallographic orientation. The onset of an antiferromagnetic ordering at 56 K features a ferromagnetic coupling within a RuO_6 bilayer, and an antiferromagnetic coupling between the neighboring bilayers. The magnetic easy axis is along the a axis for $48 < T < 56$ K, and switches to the

b axis below a structural transition for $T < 48$ K.[20] Therefore, the magnetic susceptibility along the respective in-plane axis shows pronounced anisotropy. This is indeed what we found in Fig. 2(d). With the external magnetic field applied along the long edge of each crystal, S1 shows a magnetization with a single peak at the AFM transition, while that of S2 shows a plateau for $48 < T < 56$ K. They correspond to the magnetization behaviors for $H \parallel a$ and $H \parallel b$, respectively. It is therefore evident that the optical contrast in reflection under polarized light is due to the domains formed by 90° rotation, as illustrated in Fig. 1(c).

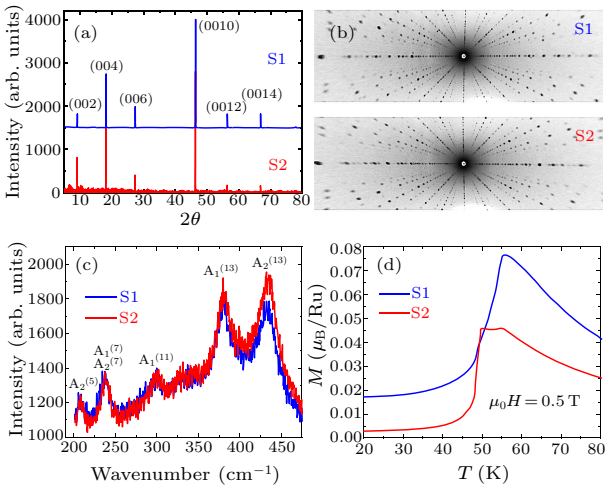

Fig. 2. (a) x-ray diffraction pattern, (b) Laue diffraction pattern, and (c) Raman spectra of $Ca_3Ru_2O_7$ crystals S1 and S2. (d) The temperature dependence of magnetization of S1 and S2, with a magnetic field of 0.5 T aligned along the long edge of each crystal.

The polarized light microscope has been used previously in crystal domain and twinning imaging,[21–23] and has been particularly useful in recent studies of electronic nematic phases.[24–26] However, the physical mechanism for showing the contrast was often overlooked. This is partly due to the complexity in human color perception, and also the different factors that contribute to the color of a material.[27] The former has been resolved by the XYZ color space[28] which correlates the color code with the color-matching function sensitive to different regions of visible wavelength. In the XYZ color space,

$$C = \int I(\lambda)R(\lambda)\bar{c}(\lambda)d\lambda, \tag{1}$$

where C is the X, Y, Z color code, λ is the wavelength, $\bar{c}(\lambda)$ is the color matching functions $[\bar{x}(\lambda), \bar{y}(\lambda), \bar{z}(\lambda)]$ that relate the spectral distribution to the color, $I(\lambda)$ is the spectral distribution of the incident light, and $R(\lambda)$ is the wavelength dependent reflectivity of the crystal. Since the color matching functions $\bar{c}(\lambda)$ are fixed, the color of the crystal depends on the incident light and the reflectivity of the crystal.

In normal incidence, the reflectivity is expressed in terms of the complex refraction index $\tilde{n}$, $R(\omega) = |\frac{\tilde{n}(\omega)-1}{\tilde{n}(\omega)+1}|^2$, with $\tilde{n}(\omega) = \sqrt{\varepsilon(\omega)}$, which depends on the complex dielectric function $\varepsilon(\omega) = \varepsilon_1(\omega) + i\varepsilon_2(\omega)$, and $\varepsilon_1(\omega)$ and $\varepsilon_2(\omega)$ are related by the Kramers–Kronig relation. There are two factors that contribute to the optical response of a metallic system, the interband and intraband transitions. The interband transition is better studied in semiconductors and can be calculated using first-principles by taking the detailed band structures into account. The intraband transition is due to the free carrier and can be conveniently modeled in the Drude theory, by $\varepsilon_2^{\text{intra}}(\omega) = \frac{\gamma\omega_p^2}{\omega(\gamma^2+\omega^2)}$, where $\omega_p = e\sqrt{4\pi n/m^*}$ is the plasma frequency, n, m^* and γ being the carrier density, carrier effective mass and relaxation time, respectively; ω_p for $Ca_3Ru_2O_7$ was found to be around 10^3 cm^{-1}.[29] The overall optical response of a metal is determined by the complex dielectric function involving both $\varepsilon^{\text{inter}}(\omega)$ and $\varepsilon^{\text{intra}}(\omega)$.

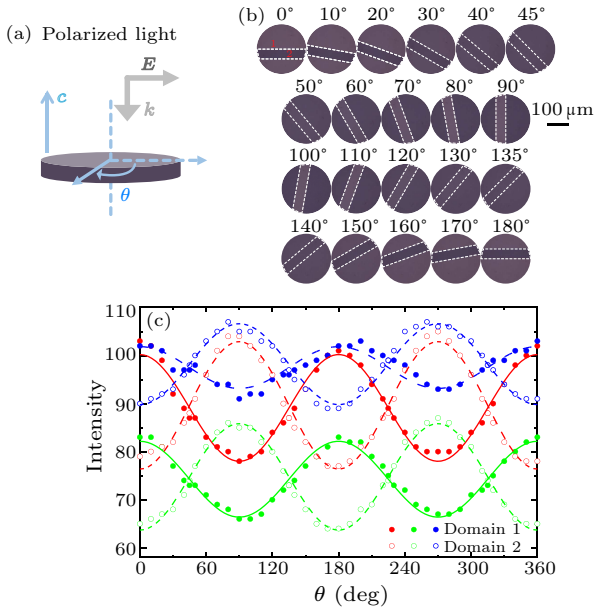

Fig. 3. (a) A schematic showing the relative orientation between the electric field orientation and the crystalline axis. (b) The polarized light images of a selected crystal featuring well defined domains. The angle θ denotes the angle between the electric field orientation and the domain wall indicated by the white dash lines. Domains 1 and 2 are marked by the red numbers. (c) The angle dependence of color of domains 1 and 2. The red, green and blue curves are the corresponding RGB values.

One advantage of the optical response of single crystalline sample is the well-defined macroscopic crystal lattice symmetry. Even without a quantitative calculation, insight can be drawn through symmetry analysis. Figure 3(a) shows the setup of the polarized light microscope, with an additional parameter, θ being the relative orientation between the electric field component of the incident light, and crystallographic a direction of $Ca_3Ru_2O_7$ crystals. We intentionally choose an area with two domains walls, marked by

the white dash lines in Fig. 3(b). The color of the domains shows apparent dependence on the relative orientation θ. It can be seen that neighboring domains change their respective color progressively, until they exchange the color at $\theta = 90°$. To see this more quantitatively, the colors of the neighboring domains are converted to their corresponding RGB color code (which can be converted conveniently to the XYZ code mentioned earlier[30]). Figure 3(c) shows the similar overall behavior for both domains (solid and open symbols), with a 90° shift between the two domains due to the 90° twined structure identified above. Each domain shows a clear two-fold symmetry of the color as a function of θ. The lattice symmetry of the crystal provides a straightforward understanding for this.

$Ca_3Ru_2O_7$ has an orthorhombic lattice in the space group of $Bb2_1m$. The dielectric tensor for such a lattice is[31]

$$\begin{pmatrix} \varepsilon_{xx} & 0 & 0 \\ 0 & \varepsilon_{yy} & 0 \\ 0 & 0 & \varepsilon_{zz} \end{pmatrix},$$

where all off-diagonal components are zero when the external electric field is along the principal crystallographic axes. In normal incidence, the electric field of the polarized light is in the ab plane. Therefore, we neglect the z component and find the intensity of the reflected light at each wavelength to be

$$\begin{aligned} I(\lambda) &= (\sin\theta \quad \cos\theta) \begin{pmatrix} \tilde{r}_x^*(\lambda) & 0 \\ 0 & \tilde{r}_y^*(\lambda) \end{pmatrix} \\ &\quad \cdot \begin{pmatrix} \tilde{r}_x(\lambda) & 0 \\ 0 & \tilde{r}_y(\lambda) \end{pmatrix} \begin{pmatrix} \sin\theta \\ \cos\theta \end{pmatrix} \\ &= \frac{1}{2}\left[|\tilde{r}_x(\lambda)|^2 + |\tilde{r}_y(\lambda)|^2 \right. \\ &\quad \left. + [|\tilde{r}_y(\lambda)|^2 - |\tilde{r}_x(\lambda)|^2]\cos(2\theta)\right]. \end{aligned}$$

Note that the $\cos(2\theta)$ term exists for each wavelength, therefore the corresponding color by Eq. (1) carries the same angle dependence, which is the two-fold rotational symmetry seen in Fig. 3(c), as shown by the solid and dashed fitting curves.

It is important to emphasize that the electronic structure of the crystal surface can be different from its bulk phase, due to the reduced symmetry of the surface compared to the bulk structure.[32] In $Ca_3Ru_2O_7$, the rotation and tilting of RuO_6 octahedra breaks the inversion symmetry of the lattice.[17] As a result, the surface of $Ca_3Ru_2O_7$ renders more subtlety. As illustrated in Fig. 4(a), the natural cleavage surface of $Ca_3Ru_2O_7$ is the bisecting plane between the RuO_6 bilayers. There are two cleavage planes, each at $z = 0.25$ and $z = 0.75$ in the unit cell. As a result, four cleavage surfaces [CS1–CS4 listed in Fig. 4(b)] can be found. Due to the mirror symmetry $(x, y, z) \rightarrow (x, y, -z)$ of the space group $Bb2_1m$, the two cleavage planes are equivalent. For the same reason, it can be found that the cleavage surfaces CS1 and CS4 are symmetrical with respect to the mirror plane of $z = 0.5$, and so are CS2 and CS3. Therefore, in our optical measurements only two cleavage surfaces are in concern, which are the opposite cleavage surfaces CS1 and CS2. A representative pair of opposite cleavage surfaces with their respective 90° domains are shown in Fig. 4(d). Under the same lighting condition, the two opposite surfaces display two different reflections. The color difference can be understood in the framework discussed above, where the difference in electronic structure of the respective surface dominates. The charge density distribution on the CS1 and CS2 planes in an infinite crystal is calculated, as shown in Fig. 4(c). Apparent difference between them can be seen, mostly due to the oxygen orbits at the apex of the tilted RuO_6 octahedra. In a realistic semi-infinite crystal, the reduced symmetry and possible surface structural reconstruction will further contribute to the observed contrast between CS1 and CS2.

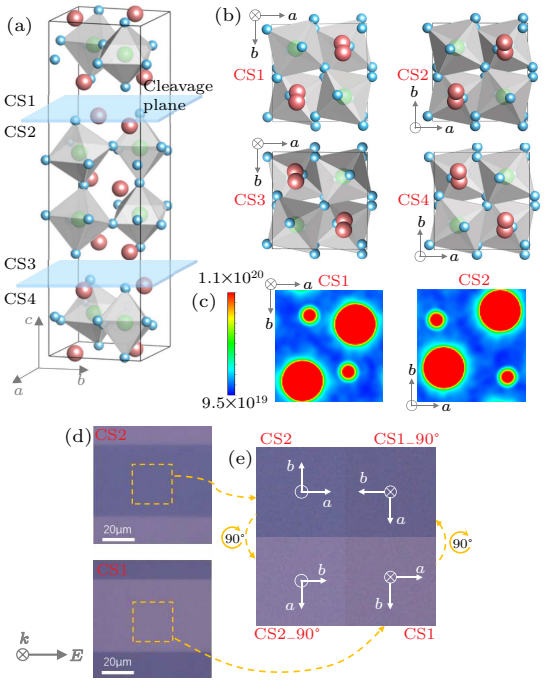

Fig. 4. (a) The crystal structure of $Ca_3Ru_2O_7$. The red, green, and blue balls stand for Ca, Ru, and oxygen, respectively. The cleavage plane ($z = 0.75c$, where c is the lattice c constant) is indicated, which is also equivalent to the plane at $z = 0.25c$. (b) The structure of the opposite cleavage surfaces, (c) the charge density distribution of surfaces CS1 and CS2. (d) The polarized light images for CS1 and CS2. (e) These two opposite cleavage surfaces and their 90°-rotated domains show four different colors, which are used for the direct determination of the crystallographic orientation of each domain. Note that the incident light intensity was intentionally increased to enhance the color contrast.

The two inequivalent surfaces CS1 and CS2 and their 90° domains lead to four different colors in total, as summarized in Fig. 4(e). It is interesting to note that these distinct colors in fact carry the information of the crystallographic orientations of their

corresponding bulk structures. Here, the incident light intensity was intentionally increased to enhance the color contrast. Through a careful comparison with the color of S1 and S2 under the same lighting condition and optical magnification, we find that upper left in Fig. 4(e) has the longer edge along the a axis, as illustrated above. It can either be CS1 or CS2, and lower left in Fig. 4(e) is either CS2 or CS1. It can be seen that CS1 and CS2 in fact correspond to the same bulk lattice. Therefore, once the four colors for the inequivalent cleavage surfaces and their 90° domains are obtained, the crystallographic orientations of all the domain are determined, as labeled in Fig. 4(e). The four different contrast serves as a color code for a direct determination of the crystallographic orientations.

The in-plane orientation dependence of the polarized light reflectance and the difference in opposite cleavage surfaces demonstrate the sensitivity of this method to the twined crystals and the intrinsic noncentrosymmetricity of the lattice. Such a structural domain imaging is not only advantageous for the use in crystal quality screening as discussed above, it is even more useful in systems where additional order coexists. For example, the possible existence of spontaneous ferroelectric domain[17] in $Ca_3Ru_2O_7$ observed using second order harmonic generation, needs to be differentiated from the structural domain due to the structural twinning. Furthermore, the capability of the direct determination of crystallographic orientation based on such a feasible polarized light imaging approach brings unprecedent efficiency and convenience in structural characterization in $Ca_3Ru_2O_7$, and may be applied in many other noncentrosymmetric materials. Other applications can also be expected in the emergence of phase separation found near the metal-insulator transitions in several ruthenate compounds, where the lattice degree of freedom is believed to be essential.[33–35]

In summary, our results demonstrate an efficient and feasible imaging of the domains in noncentrosymmetric $Ca_3Ru_2O_7$ crystals using polarized light reflection at normal incidence. The difference in reflection at domains with orthogonal in-plane orientations in $Ca_3Ru_2O_7$ provides a clear contrast for the imaging. Furthermore, the color contrast between all inequivalent cleavage surfaces is found to be a color code for the direct determination of the crystallographic orientation of each domain. Such an approach provides an efficient yet feasible method for structural domain characterization in $Ca_3Ru_2O_7$, which can also find applications in noncentrosymmetric crystals in general.

Hui Xing acknowledges Zhiwen Shi and Hao Zeng for useful discussions.

References

[1] Cheng J G, Zhou J S, Goodenough J B and Jin C Q 2012 *Phys. Rev. B* **85** 184430
[2] Perry R S *et al.* 2001 *Phys. Rev. Lett.* **86** 2661
[3] Sokolov D A *et al.* 2019 *Nat. Phys.* **15** 671
[4] Borzi R A, Grigera S A, Farrell J, Perry R S, Lister S J S, Lee S L, Tennant D A, Maeno Y and Mackenzie A P 2007 *Science* **315** 214
[5] Lester C *et al.* 2015 *Nat. Mater.* **14** 373
[6] Mackenzie A P and Maeno Y 2003 *Rev. Mod. Phys.* **75** 657
[7] Pustogow A *et al.* 2019 *Nature* **574** 72
[8] Mizokawa T, Tjeng L H, Sawatzky G A, Ghiringhelli G, Tjernberg O, Brookes N B, Fukazawa H, Nakatsuji S and Maeno Y 2001 *Phys. Rev. Lett.* **87** 077202
[9] Nakamura F, Sakaki M, Yamanaka Y, Tamaru S, Suzuki T and Maeno Y 2013 *Sci. Rep.* **3** 2536
[10] Cao G, McCall S, Crow J E and Guertin R P 1997 *Phys. Rev. Lett.* **78** 1751
[11] Xing H *et al.* 2018 *Phys. Rev. B* **97** 041113(R)
[12] Horio M *et al.* 2019 arXiv:1911.12163 [cond-mat.str-el]
[13] Puggioni D, Horio M, Chang J and Rondinelli J M 2020 *Phys. Rev. Res.* **2** 023141
[14] Markovic I *et al.* 2020 *Proc. Natl. Acad. Sci. USA* **117** 15524
[15] Yoshida Y, Ikeda S I, Matsuhata H, Shirakawa N, Lee C H and Katano S 2005 *Phys. Rev. B* **72** 054412
[16] Jin Z and Ku W 2018 arXiv:1809.04589 [cond-mat.str-el]
[17] Lei S *et al.* 2018 *Nano Lett.* **18** 3088
[18] Cao G and Schlottmann P 2008 *Mod. Phys. Lett. B* **22** 1785
[19] Iliev M N, Jandl S, Popov V N, Litvinchuk A P, Cmaidalka J, Meng R L and Meen J 2005 *Phys. Rev. B* **71** 214305
[20] Fobes D, Peng J, Qu Z, Liu T J and Mao Z Q 2011 *Phys. Rev. B* **84** 014406
[21] Weightman P, Martin D S, Cole R J and Farrell T 2005 *Rep. Prog. Phys.* **68** 1251
[22] Kaminsky W, Claborn K and Kahr B 2004 *Chem. Soc. Rev.* **33** 514
[23] Rubio-Marcos F, Del Campo A, Marchet P and Fernández J F 2015 *Nat. Commun.* **6** 6594
[24] Chu J H, Analytis J G, De Greve K, McMahon P L, Islam Z, Yamamoto Y and Fisher I R 2010 *Science* **329** 824
[25] Tanatar M A *et al.* 2016 *Phys. Rev. Lett.* **117** 127001
[26] Tanatar M A, Kreyssig A, Nandi S, Ni N, Bud'ko S L, Canfield P C, Goldman A I and Prozorov R 2009 *Phys. Rev. B* **79** 180508(R)
[27] Xue Y, Zhang Y and Zhang P H 2009 *Phys. Rev. B* **79** 205113
[28] Smith T and Guild J 1931 *Trans. Opt. Soc.* **33** 73
[29] Lee J S, Moon S J, Yang B J, Yu J J, Schade U, Yoshida Y, Ikeda S I and Noh T W 2007 *Phys. Rev. Lett.* **98** 097403
[30] Fairman H S, Brill M H and Hemmendinger H 1997 *Color Res. Appl.* **22** 11
[31] Hutchings D C 2004 *Applied Nonlinear Optics* (Glasgow: University of Glasgow)
[32] Plummer E W, Ismail, Matzdorf R, Melechko A V, Pierce J P and Zhang J D 2002 *Surf. Sci.* **500** 1
[33] Kim T H, Angst M, Hu B, Jin R, Zhang X G, Wendelken J F, Plummer E W and Li A P 2010 *Proc. Natl. Acad. Sci. USA* **107** 5272
[34] Zhang J *et al.* 2019 *Phys. Rev. X* **9** 011032
[35] Gangshettiwar A, Zhu Y, Jiang Z, Peng J, Wang Y, He J, Zhou J, Mao Z and Lai K 2020 *Phys. Rev. B* **101** 201106